frontiers | Frontiers in Sensors

TYPE Original Research
PUBLISHED 16 December 2024
DOI 10.3389/fsens.2024.1508810

OPEN ACCESS

EDITED BY
Marcela Cecilia Rodríguez,
National University of Cordoba, Argentina

REVIEWED BY
Xinxin Xiao,
Aalborg University, Denmark
Diego Pallarola,
National University of General San Martín, Argentina

*CORRESPONDENCE
Juliana Cancino-Bernardi,
jucancino@usp.br
Claudia do Amaral Razzino,
claudiarazzino@gmail.com

†These authors have contributed equally to this work

RECEIVED 09 October 2024
ACCEPTED 26 November 2024
PUBLISHED 16 December 2024

CITATION
Razzino CdA, Sgobbi LF, Cancino-Bernardi J, Zapata AMM, Costa CC, Zucolotto V, Vieira L and Lobo AO (2024) A microbead-enhanced electrochemical platform for β-amyloid peptide (1–42) detection.
Front. Sens. 5:1508810.
doi: 10.3389/fsens.2024.1508810

A microbead-enhanced electrochemical platform for β-amyloid peptide (1–42) detection

Claudia do Amaral Razzino[1,2*†], Lívia Flório Sgobbi[3†], Juliana Cancino-Bernardi[4*†], Angelica Maria Mazuera Zapata[2], Clara Cardoso Costa[4], Valtencir Zucolotto[2], Lucia Vieira[1] and Anderson Oliveira Lobo[5]

[1]Research and Development Institute, University of Vale do Paraiba, São José dos Campos, Brazil, [2]Nanomedicine and Nanotoxicology Group, Sao Carlos Institute of Physics, University of Sao Paulo, Sao Carlos, Brazil, [3]Institute of Chemistry, Federal University of Goias, Goiania, Brazil, [4]Department of Chemistry, Faculty of Philosophy, Sciences and Letters of Ribeirao Preto, University of Sao Paulo, Ribeirao Preto, Brazil, [5]Interdisciplinary Laboratory for Advanced Materials, Federal University of Piaui, Teresina, Brazil

Alzheimer's disease is the most prevalent form of dementia and is primarily characterized by the accumulation of β-amyloid and phosphorylated tau proteins in the brain, along with the degeneration of nerve cells, which leads to impairment of various cognitive functions. A significant biomarker of Alzheimer's disease is the decreased level of soluble β-amyloid peptide (1–42) ($A\beta_{1\text{-}42}$) in cerebrospinal fluid (CSF), as pathology progresses when CSF-$A\beta_{1\text{-}42}$ levels drop below 192 pg mL^{-1}. In this study, we developed an amperometric immunosensor based on magnetic beads as the platform for constructing the immunosensor. Monoclonal antibodies are immobilized on the MBs, enabling selective detection of $A\beta_{1\text{-}42}$. The detection antibody is conjugated with the enzyme horseradish peroxidase, which, in the presence of H_2O_2 and hydroquinone, catalyzes the decomposition of H_2O_2 and the oxidation of hydroquinone to p-quinone, generating an electric current measured at a potential of −200 mV (vs. the Ag pseudo-reference electrode) using screen-printed carbon electrodes. The amperometric sandwich-type immunosensor demonstrates a linear response in the concentration range of 10 to 10,000 pg mL^{-1}, with a detection limit of 7.4 pg mL^{-1}, exhibiting excellent selectivity against the assessed interferents. These findings suggest the potential application of this immunosensor in the early diagnosis of Alzheimer's disease, offering a sensitive and specific tool for clinical analysis. Despite its high performance, further studies are required to validate its robustness and applicability in complex clinical samples.

KEYWORDS

screen-printed electrode, magnetic beads, amperometric immunosensor, amperometric sandwich immunoassay, β-amyloid peptide (1–42)

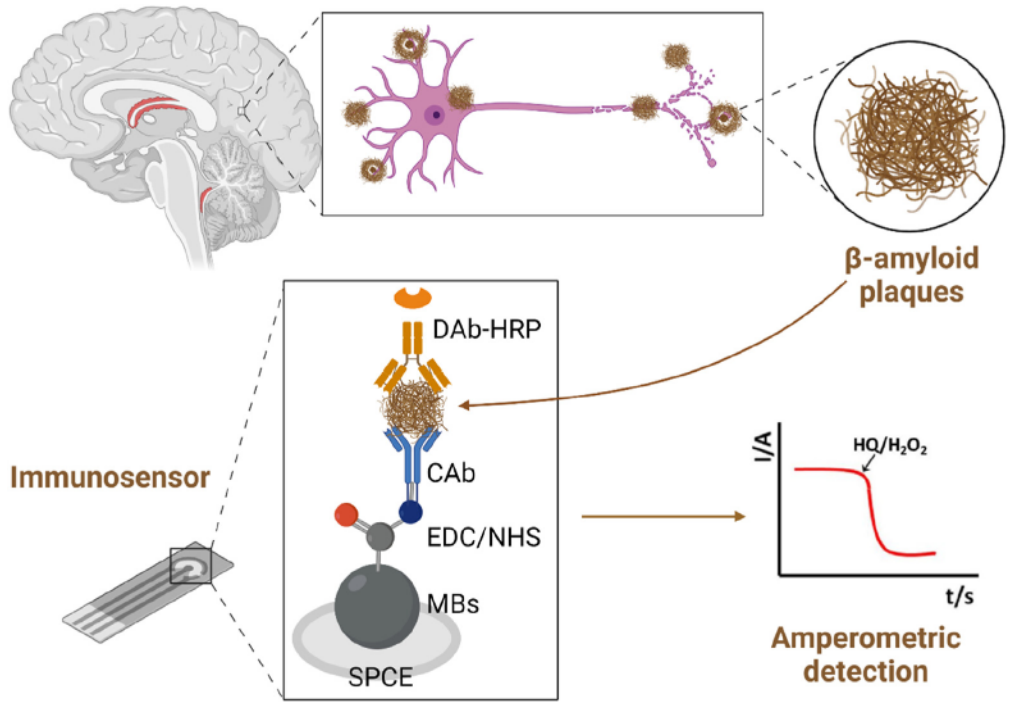

GRAPHICAL ABSTRACT

1 Introduction

The term dementia, as defined by the World Health Organization, encompasses various progressive diseases that impair memory, cognitive abilities, and behavior, significantly diminishing an individual's ability to perform daily activities. Alzheimer's disease (AD) is the most prevalent form of dementia, accounting for 60%–70% of cases (WHO, 2017). AD is primarily characterized by the accumulation of β-amyloid and phosphorylated tau proteins in the brain, along with the degeneration of nerve cells. These processes significantly impact various cognitive functions (Findeis, 2007; Zaretsky et al., 2022). The accumulation of β-amyloid plaques and oligomers can damage neurons by interfering with synapses. β-amyloid peptide (1–42) ($A\beta_{1-42}$) constitutes the main component of β-amyloid plaques found in the brains of individuals with AD. Early in sporadic AD, the levels of $A\beta_{1-42}$ in the cerebrospinal fluid (CSF) increase, but they decrease as the disease progresses, indicating aggregation and deposition of $A\beta_{1-42}$ (Findeis, 2007). A crucial biomarker of AD is the decreased levels of soluble $A\beta_{1-42}$ in CSF, coupled with the amyloid load, which suggests an elevated intratissue amyloid removal rate (Zaretsky et al., 2022; Alex and Gunn, 2019).

Conventional methods like enzyme-linked immunosorbent assays (ELISA) are typically employed to quantify $A\beta_{1-42}$ levels in CSF. However, they are labor-intensive, time-consuming, require costly reagents, are susceptible to false positives, and lack sensitivity to low biomarker levels (Shui et al., 2018). In this context, there is a critical need for highly sensitive, accessible, and cost-effective methods that can deliver fast and reliable results. In response to this demand, electrochemical biosensors have emerged as a powerful analytical tool that meets these criteria (Serafín et al., 2020; Brazaca et al., 2020; Toyos-Rodríguez et al., 2020). Electrochemical immunosensors offer advantages for field analysis due to their miniaturization and portability, rapid detection from the electroanalytical response, and cost reduction from the small quantities of reagents and samples required. They are also easy to operate by untrained users, and potentiostats, in contrast to ELISA readers, are simpler in construction and have a more accessible final cost.

Affinity ligand-based electrochemical biosensors offer rapid, simple, and sensitive analysis of AD biomarkers, including $A\beta_{1-42}$ (Le et al., 2020; Wang et al., 2023). One effective strategy to achieve high signal-to-background ratios and enhance sensor sensitivity is sandwich-like configurations (Serafín et al., 2020). Additionally, the use of monoclonal antibodies in immunosensors enhances selectivity by capturing the target with precision.

In this context, we introduce a magnetic bead-based electrochemical immunosensor utilizing a sandwich-like configuration for $A\beta_{1-42}$ detection using screen-printed carbon electrodes (SPCE). This strategy eliminates the need for exhaustive preparation steps. The sensor interface is swiftly and directly constructed onto commercial magnetic microbeads, which are then magnetically immobilized on the SPCE. Furthermore, the amperometric signal is generated using horseradish peroxidase enzyme (HRP) as a label for the secondary antibodies, with hydroquinone (HQ) serving as an effective electron mediator for the reduction reaction of H_2O_2. In this way, the construction of the sensor interface, which requires blocking steps, and the biorecognition reactions occurring on the surface of the MBs leave the transducer free to facilitate electron transfer from the HRP/H_2O_2/HQ system, without compromising the immunosensor's sensitivity (Conzuelo et al., 2012a).

2 Experimental

2.1 Reagents and solutions

Screen-Printed Carbon Electrodes (Ref. 110) were purchased from Metrohm DropSens. Hydrophilic Dynabeads™ with carboxylic acid groups (MBs, Ø = 2.8 μm, Ref. 14305D) were purchased from Invitrogen-Thermo Fisher. N-(3-dimethylaminopropyl)-N′-ethylcarbodiimide (EDC), N-hydroxysulfosuccinimide (NHSS), ethanolamine (ETA), hydroquinone (HQ), and hydrogen peroxide (H_2O_2) (30%, v/v) were purchased from Sigma-Aldrich. Blocking Buffer (BB) Pierce™ Protein-Free (Ref. 37572) was purchased from Thermo Scientific. Human β-Amyloid Peptide (1–42) (Ref. 932502), Purified anti-β-Amyloid 1–42 Antibody (Ref. 805501, used as the capture antibody, CAb) and HRP anti-β-Amyloid 1–16 Antibody (Ref. 803012, used as the detection antibody, DAb-HRP) were purchased from BioLegend Inc. All solutions were prepared with ultrapure water from a Millipore Milli-Q water purification system (18.2 MΩ cm). Phosphate-buffered saline (PBS) (NaCl 137 mmol L^{-1} and KCl 2.7 mmol L^{-1}) pH 7.4 and pH 8.0; phosphate buffer 0.05 mol L^{-1}, pH 6.0; phosphate buffer 0.1 mol L^{-1}, pH 8.0; MES buffer 25 mmol L^{-1}, pH 5.0 and Tris-HCl buffer 0.1 mol L^{-1}, pH 7.4. All reagents were of analytical grade and were used without further purification.

2.2 Characterization of the immunosensor platform

In the process of constructing sensing interfaces on magnetic microparticles, an Agimaxx Thermoshaker, model AG-100R, was utilized for the incubation steps, while a Gehaka vortex, model AV-2, was employed to solubilize the dispersions. Magnetic separation during the incubation and washing processes of the magnetic microparticles was carried out using a DynaMag™-2 magnet (Invitrogen-Thermo Fisher). The capture of modified magnetic microparticles onto the surface of the working electrode (SPCE) was achieved using a homemade polymethylmethacrylate (PMMA)-coated holding block with an encapsulated neodymium magnet (AIMAN GZ), which holds the SPCE electrode.

The chronoamperometry measurements were conducted using a PGSTAT 302N potentiostat/galvanostat from Autolab® (Eco Chemie, Netherlands) connected to a microcomputer running NOVA software (version 2.1.3 - Metrohm Autolab B.V., Netherlands). All electrochemical measurements were carried out at room temperature in a 15 mL electrochemical cell with a SPCE working electrode, Ø = 5 mm.

The modification of magnetic beads (MBs) was characterized before and after each step of immunosensor construction. Dynamic Light Scattering (DLS) was utilized to assess the hydrodynamic diameter and distribution of the samples in suspension. The measurements were conducted in triplicate at room temperature using a Malvern spectrometer Nano-ZS (Malvern Instruments), model ZEN3601. Additionally, the zeta potential of the MBs after each functionalization step was evaluated using the same DLS equipment. The results are reported as mean ± standard deviation (SD) based on three independent measurements.

Transmission Electron Microscopy (TEM) images were obtained using JEOL JEM-100CXII equipment.

Infrared spectra were recorded using a Nicolet IS20 FTIR spectrometer (Thermofisher, United States) with a nitrogen gas purge. The spectral resolution was set at 4.0 cm^{-1}, and they were recorded with 64 scans in transmission mode, covering the wavenumber range of 500–4,000 cm^{-1}. Samples (5 μL) were placed on a silicon wafer ($Si/SiO_2/B$) and dried under vacuum conditions. The measurements were conducted at room temperature immediately after drying, with constant purging and a corrected background. The overall spectra were normalized.

Raman spectra were recorded using the Renishaw micro-Raman spectroscopy system in the 500–1800 cm^{-1} range (static mode) with a 532 nm laser excitation wavelength. The exposure time was set to 1 s, and 50 scans were accumulated (total exposure time of 50 s). The incident laser light was adjusted to 1% power to avoid excessive heating and fluorescence of the sample. Each sample (5 μL) was placed on a silicon wafer ($Si/SiO_2/B$) and dried under vacuum conditions. Raman spectra were collected at room temperature after drying the sample and calibrated using the silicon peak. Data processing included background subtraction and eleven-order polynomial fitting for fluorescence background removal, followed by normalization.

2.3 Immunosensors fabrication

The amperometric immunosensor was constructed using magnetic beads (MBs) as a platform to immobilize monoclonal antibodies selective for Aβ1-42. The detection antibody is conjugated to the enzyme horseradish peroxidase (HRP), which reacts with hydrogen peroxide (H_2O_2). Thus, amperometric transduction was performed on screen-printed carbon electrodes (SPCE) using the hydroquinone (HQ)/H_2O_2 system.

All incubation steps were performed in a thermoshaker operating at 950 rpm and 25°C. After each incubation, the microtubes were placed in a magnetic separator for 4 min, and then the supernatant was discarded. Initially, a 5 μL aliquot of hydrophilic beads with carboxylic acid groups was placed in a 1.5 mL microtube. Then, 50 μL of MES buffer was added and incubated for 5 min; the supernatant was removed, and the washing step was repeated. In the second step, the carboxyl groups on the surface of the magnetic beads (–COOH-MBs) were activated with EDC/NHSS by incubating in 25 μL of a 100 mmol L^{-1} EDC/NHSS solution prepared with MES buffer for 35 min. The activated –COOH-MBs were washed twice with 50 μL of MES buffer. For covalent immobilization of capture antibodies (CAb), the activated MBs were resuspended in 25 μL of a 10 μg mL^{-1} CAb solution prepared in MES buffer for 60 min. The CAb-modified MBs were washed twice with 50 μL of MES buffer. Any activated –COOH-MBs that did not react with CAb were blocked by incubation in 25 μL of a 50 mmol L^{-1} ethanolamine solution prepared in PBS (pH 8.0) for 60 min. The CAb-modified MBs were washed once with 50 μL of Tris-HCl buffer and twice with 50 μL of commercial blocking buffer solution (BB).

The detection protocol consists of incubating the MBs modified with capture antibodies (CAbs) in 25 μL of solutions of varying concentrations of $Aβ_{1-42}$ and 0.5 μg mL^{-1} of the detection antibody labeled with the enzyme horseradish peroxidase (HRP) (DAb-HRP), prepared in blocking buffer (BB), for 60 min. For amperometric

detection, the MBs modified with the immunocomplexes were washed twice with 50 μL of BB and then resuspended in 50 μL of the electrolyte, which is a 50 mmol L^{-1} sodium phosphate buffer (pH 6.0).

2.4 Amperometric sensing

The SPCEs were embedded in the PMMA block, and 50 μL of the suspension of MBs modified with the immunocomplex was magnetically captured by the magnet embedded in the block in a simple, reproducible, and stable manner (Gamella et al., 2020). The block-SPCE assembly was then immersed in an electrochemical cell containing 10 mL of 50 mmol L^{-1} phosphate buffer (pH 6.0), which contained 1.0 mmol L^{-1} of hydroquinone (HQ) (freshly prepared) (Conzuelo et al., 2012a). Amperometric measurements were conducted in solutions under magnetic stirring by applying a detection potential of −200 mV (vs. the Ag pseudo-reference electrode) (Gamella et al., 2012). The current was recorded upon reaching a steady state before (B) and after (S) the addition of 50 μL of a 0.1 mol L^{-1} hydrogen peroxide (H_2O_2) solution. The amperometric response of the immunosensor corresponds to the difference between the steady-state currents (S−B). The S−B values reported in this study are the mean of three measurements, and the error bars represent three times the standard deviation of the triplicates. Confidence intervals were calculated at a significance level of $\alpha = 0.05$.

3 Results and discussion

In the construction of the immunosensors, the carboxyl groups (−COOH) on the surface of the magnetic beads (MBs) were initially activated in EDC/NHSS solution. Next, the capture antibody (CAb) was covalently immobilized on the MBs through the interaction between the −COOH groups activated by EDC/NHSS and the amino groups of the CAb. $A\beta_{1\text{-}42}$ was then captured and "sandwiched" between the capture antibody and the detection antibody labeled with the enzyme horseradish peroxidase (HRP) (DAb-HRP). Amperometric detection was performed using screen-printed carbon electrodes (SPCEs) as transducers, where the MBs modified with the immunocomplex were magnetically immobilized using a block equipped with a magnet. Quantification of $A\beta_{1\text{-}42}$ was performed by monitoring the amperometric current at −200 mV (vs. Ag pseudo-reference) using the H_2O_2/hydroquinone (HQ) system (Volpe et al., 1998; Camacho et al., 2007). The amperometric current values obtained were proportional to the concentration of $A\beta_{1\text{-}42}$.

3.1 Characterization of the immunosensor platforms

The size and surface charge of the magnetic beads (MBs) modified with the capture antibodies (MBs-COOH-CAb) and the immunocomplex (MBs-COOH-CAb@peptide-DAb-HRP) were investigated using dynamic light scattering, zeta potential

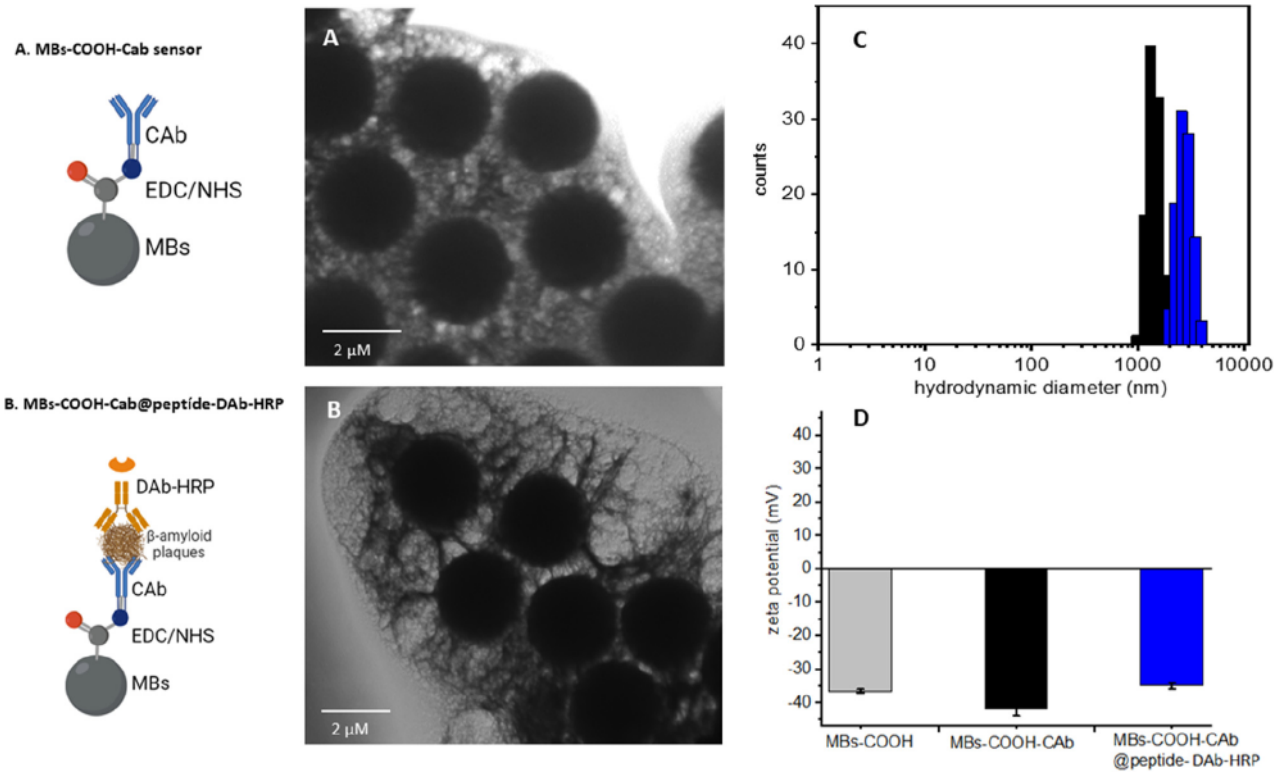

FIGURE 1
TEM images of **(A)** MBs-COOH-CAb; **(B)** MBs-COOH-CAb@peptide-DAb-HRP; **(C)** Hydrodynamic diameter obtained by DLS for (black) MBs-COOH-CAb and (blue) MBs-COOH-CAb@peptide-DAb-HRP; **(D)** Zeta potential values of (gray) MBs-COOH after washes with MES, (black) MBs-COOH-CAb and (blue) MBs-COOH-CAb@peptide-DAb-HRP.

TABLE 1 Size, polydispersive index (PdI), zeta potential and conductivity values of different steps of MBs-COOH, MBs-COOH-CAb and MBs-COOH-CAb@peptide-DAb-HRP.

Sample	Size (nm)	PdI	Zeta potential (mV)	Conductivity (mS/cm)
MBs-COOH	2793 ± 105	0.202 ± 0.05	−37 ± 1	0.011 ± 0.005
MBs-COOH-CAb	1832 ± 127	0.503 ± 0.05	−42 ± 2	0.869 ± 0.031
MBs-COOH-CAb @peptide-DAb-HRP	2095 ± 300	0.430 ± 0.06	−35 ± 1	0.781 ± 0.026

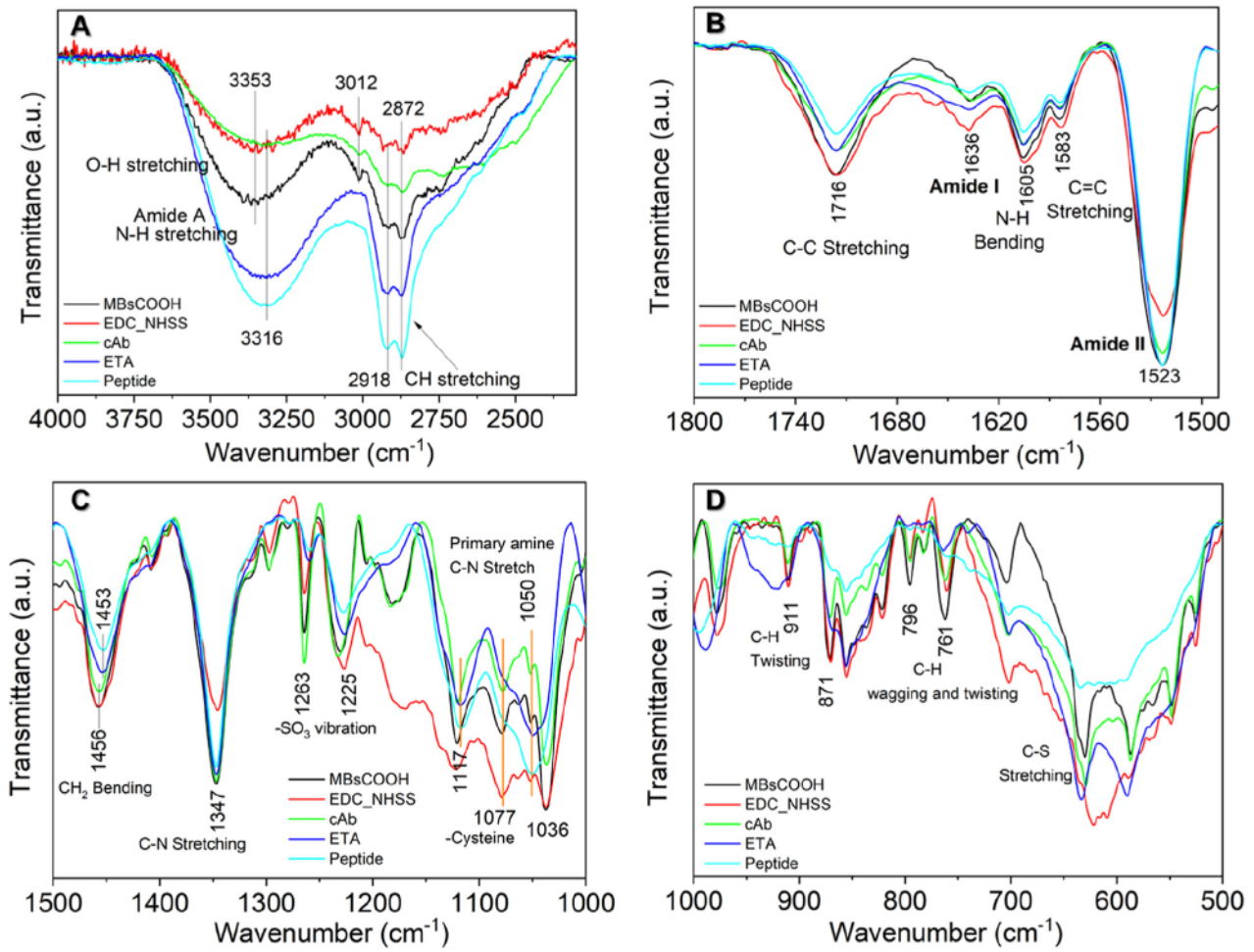

FIGURE 2
FTIR spectra MBs for each functionalization step: (black) MBs-COOH after washes with MES; (red) MBs-COOH actived with EDC-NHSS; (green) MBs-COOH-CAb; (blue) MBs-COOH-CAb after ETA and (cyan) MBs-COOH-CAb@peptide-DAb-HRP. **(A)** single bond region, **(B)** double bond region, **(C, D)** fingerprint region.

measurements, and transmission electron microscopy (TEM) images, as shown in Figure 1 and Table 1.

As shown in Figures 1C, D and Table 1, the magnetic microparticles exhibited a mean size of 2.8 ± 0.1 μm (according to the manufacturer's specifications) and a charge of −37 ± 1 mV without any pretreatment, as measured by dynamic light scattering (DLS) and zeta potential, respectively. The introduction of EDC/NHSS and capture antibody (CAb) molecules to the magnetic beads (MBs) affected the size, reducing it to 1.8 ± 0.1 μm, and the charge to −42 ± 2 mV, corresponding to a decrease of approximately 1.0 μm in size and 5 mV in charge. The surface charge and hydration layer are the main factors to contribute with this fact since MBs are often surrounded by a hydration layer or an electric double layer in a liquid medium. When antibodies are attached to the surface, the zeta potential of the NP changes, altering the structure or thickness of this layer, which might result in a smaller effective hydrodynamic diameter being measured, as observed in our DLS results that decrease from 2,793 ± 105 to 1832 ± 127 nm. Moreover, some NPs come with a stabilizing layer like polymers or surfactants that maintain their stability and prevent aggregation. During antibody

conjugation, this layer may be partially or completely replaced by the antibody molecules, resulting in a net decrease in overall particle size. These changes were also reflected in the conductivity profile, which significantly increased from 0.011 to approximately 0.800 m/cm after the MBs' surface modification and by an increase in polydispersity index (PdI) values from 0.202 to 0.503.

The biorecognition step was evidenced by a slight variation in the zeta potential values, changing from −42 ± 2 to −35 ± 1 mV due to the incorporation of @peptide-DAb-HRP onto the MBs-COOH-CAb, as well as an increase in size of approximately 0.3 µm. These changes were expected due to the presence of biomolecules on the protein/peptide surface contributing to the surface charge. Transmission electron microscopy (TEM) images further confirmed the modification steps (Figures 1A, B). The soft pattern observed around the magnetic microparticles is attributed to the presence of biological molecules on the surface.

The interaction of magnetic beads (MBs) with modifiers at each stage of the immunosensor construction was analyzed using Fourier-transform infrared spectroscopy (FTIR), as shown in Figure 2.

Initially, FTIR spectra were obtained for as-received MBs-COOH and compared with MBs-COOH washed with MES buffer. Figures 2–A displays the typical functional groups associated with the MBs-COOH surface structure for both samples. In the single bond region (4,000–2,500 cm^{-1}), O–H bending modes at 3,307 cm^{-1} and C–H stretching with a broad band at 2,921 cm^{-1} were observed. Figures 2–B shows the double bond region (2,000–1,500 cm^{-1}) associated with C–C and C=C stretching modes, as well as N–H bending from lipids, esters, amide I, and amide II bands (Miller et al., 2013; Burt et al., 2004). Notably, three main bands were observed at 1716, 1,605, and 1,523 cm^{-1}, corresponding to C–C stretching, N–H bending, and C=C stretching, respectively, from the MBs-COOH (Byun, 2016). Figures 2–C, D highlight the main differences in the spectra in the region from 1,500 to 500 cm^{-1}. Two primary bands were observed at 1,456 cm^{-1} and 1,347 cm^{-1}, corresponding to the C–H_2 bending and C–N stretching modes, respectively. Additionally, bands at 1,263 and 1,225 cm^{-1} may represent the SO_3 vibration and residues from cysteine at 1,077 cm^{-1} (Miller et al., 2013; Burt et al., 2004; Byun, 2016).

The second step in the construction of the immunosensor consists of activating the –COOH groups on the MBs with EDC/NHSS to facilitate the covalent immobilization of the capture antibody. This activation was characterized by a decrease in the intensity of the band at 3,353 cm^{-1}, which is related to the N–H stretching mode. The decrease occurred due to the reaction of N–H groups with EDC/NHSS, forming secondary amine bonds in the same region as the O–H stretching band (Byun, 2016). The immobilization of the capture antibody (CAb) was evidenced by a decrease in the band intensity associated with primary amine stretching groups in the range of 1,500 to 1,050 cm^{-1}. This reduction is likely caused by the rearrangement of the amino acids in the monoclonal antibody CAb with the carboxylic acid C=O, which results in a decrease in the total dipole moment, as described in the literature (Moran and Zanni, 2014).

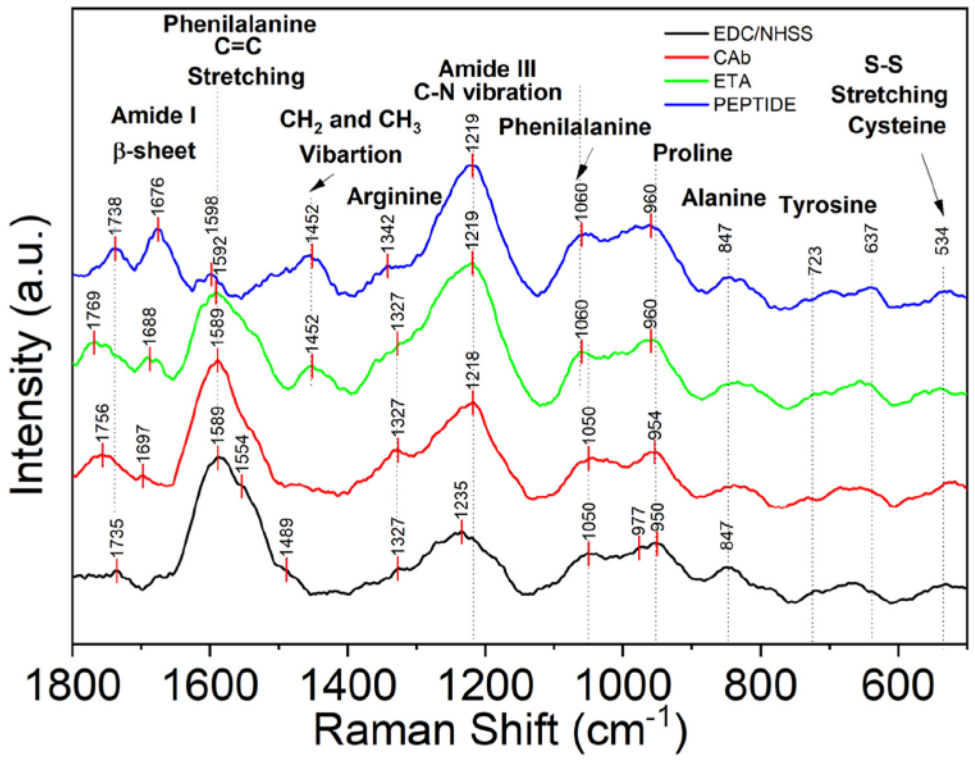

FIGURE 3
Raman spectra in the Fingerprint region (1800–500 cm^{-1}) for each functionalization step: (black) MBs-COOH actived with EDC-NHSS incubation; (red) MBs-COOH-CAb; (green) MBs-COOH-CAb stabilized with ETA and (blue) MBs-COOH-CAb@peptide-DAb-HRP.

The blocking step with ethanolamine (ETA) was confirmed by an increase in the band intensities in the regions corresponding to O–H, N–H, and C–H stretching modes, attributed to the presence of amine and hydroxyl groups in the ETA molecule. Finally, the cyan spectrum in Figure 2 revealed the biorecognition step of the complex composed of the peptide bound to the detection antibody labeled with the HRP enzyme and captured by the capture antibody immobilized on the MBs. Studies from the literature have demonstrated the presence of native β-amyloid by the existence of primary amide bands and anti-parallel β-sheet structures between 1,630–1,643 cm^{-1} and 1,670–1,695 cm^{-1}, respectively (Moran and Zanni, 2014; Zandomeneghi et al., 2004; Sarroukh et al., 2013; Boelens et al., 2022). The stretching band between 1,650 and 1,658 cm^{-1} is indicative of an α-helical structure, while the band at 1,644 cm^{-1} is related to random coil structures in the secondary protein structure. Consequently, the broad band around 1,636 cm^{-1} may be associated with β-sheet proteins and primarily arises from the C=O stretching vibration with a minor contribution from C–N stretch (Miller et al., 2013; Sarroukh et al., 2013; Boelens et al., 2022; Breydo et al., 2016). In a β-sheet, the normal modes are delocalized both along and across the structure, and its frequency provides information on its size and rigidity (Moran and Zanni, 2014;

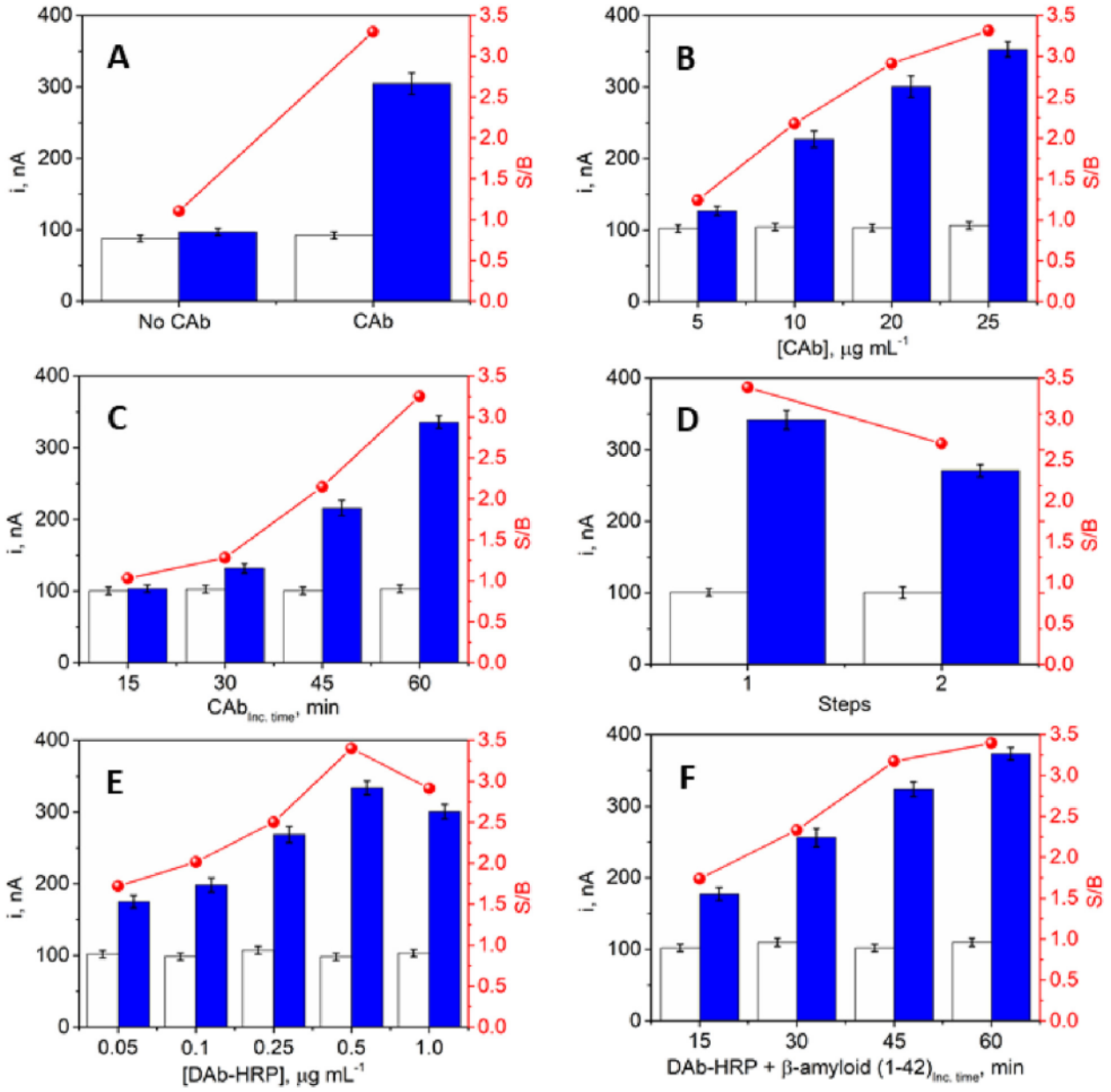

FIGURE 4
(A) Feasibility of the immunoassay and **(B–F)** the impact of various working variables on the amperometric response; **(B)** concentration of the capture antibody (CAb) and **(C)** incubation time of CAb; **(D)** steps involved in the working protocol; **(E)** concentration of the mixture [$Aβ_{1-42}$ + detection antibody-HRP (DAb-HRP)], and **(F)** incubation time of $Aβ_{1-42}$ + DAb-HRP. The amperometric responses measured in the presence of 0.0 (white bars) and 5.0 (blue bars) ng mL^{-1} of $Aβ_{1-42}$ are presented, along with the resulting signal-to-blank ratios (S/B) represented by red dots and lines.

Zandomeneghi et al., 2004; Sarroukh et al., 2013; Guivernau et al., 2016).

In addition to the FTIR studies, Raman spectroscopy was used to gather further information on the interaction of MBs with the modifiers at each stage of immunosensor construction, as illustrated in Figure 3.

The characteristic peaks from MBs-COOH are observed around 1,060 and 1,600 cm^{-1}, corresponding to aliphatic and aromatic C–C stretching vibrations from the carboxylic groups on the MBs' surface, corroborating the FTIR results (van Apeldoorn et al., 2005). Additionally, the immunocomplex MBs-COOH-CAb@peptide-DAb-HRP exhibited two peaks in the same region, corresponding to the benzene ring breathing and C=C vibration associated with phenylalanine, an amino acid present in the protein complex (Imanbekova et al., 2021; Ishigaki et al., 2020). Confirming these findings, a peak at 1,235 cm^{-1} was observed, corresponding to the stretching mode of C–C_6H_5 of phenylalanine (Ishigaki et al., 2020). The presence of CAb on the MB particles was confirmed by the peak at 1,688 cm^{-1} (amide I), which can be assigned to C=O and a minor contribution of C–N stretching. These peaks increased in intensity after peptide biorecognition on the surface of the MBs-COOH-CAb (Boelens et al., 2022; Imanbekova et al., 2021; Ishigaki et al., 2020; Chen et al., 2015; Michael et al., 2014). The peptide backbone is also observed at 1,452 cm^{-1}, attributed to CH_3 deformation and a ternary amide belonging to the N–H bend (Ishigaki et al., 2020; Michael et al., 2014). This peak emerges with the presence of biomolecules CAb and $A\beta_{1\text{-}42}$ peptide. Furthermore, other peaks in the spectra were attributed to residues of specific amino acids, including a tyrosine doublet at 723 and 637 cm^{-1}, alanine at 847 cm^{-1}, proline at 950 cm^{-1}, and cysteine at 534 cm^{-1} (Burt et al., 2004; Boelens et al., 2022; Imanbekova et al., 2021; Ishigaki et al., 2020). The cysteine residues in CAb must be free to interact and couple with the –COOH groups of MBs, consistent with the analysis of FTIR spectra (Burt et al., 2004; Boelens et al., 2022; Michael et al., 2014).

3.2 Optimizing the experimental variables

The experimental variables at each step of the sandwich amperometric immunosensor construction were optimized by considering the amperometric responses of both unmodified and CAb-modified MBs, in the absence (B) of the $A\beta_{1\text{-}42}$ standard and in the presence (S) of 5.0 ng mL^{-1} of the $A\beta_{1\text{-}42}$ standard, along with the corresponding S/B ratio values. The same conditions and reagents were used for both S and B measurements to ensure that any variation in the S/B ratio was solely attributable to the presence or absence of $A\beta_{1\text{-}42}$. Figures 4–A demonstrates that there is no nonspecific adsorption of $A\beta_{1\text{-}42}$ and DAb-HRP in the absence of CAb, thus confirming the functionality and feasibility of the proposed sandwich immunoassay.

The crucial experimental variables for the preparation of the sandwich amperometric immunosensor were optimized. The comparison of the signal-to-blank ratio values (S/B) corresponding to the amperometric current measured in the absence (B) and presence (S) of 5.0 ng mL^{-1} of $A\beta_{1\text{-}42}$ was used to determine the optimal variable values for each step. The amount of magnetic microbeads (5 µL) used aligns with that reported in the literature (Conzuelo et al., 2012b; Eguílaz et al., 2010). The use of 50 mM ethanolamine as a blocking solution follows the manufacturer's protocol for Dynabeads® M-270 Carboxylic Acid (MBs). According to the study by Eguiláz et al. (Eguílaz et al., 2010), the reduction potential for the decomposition of H_2O_2 in the HRP/H_2O_2/HQ system using a 0.05 mol L^{-1} sodium phosphate buffer electrolyte at pH 6.0 should be −200 mV to achieve good sensitivity and accuracy in the amperometric response (Gamella et al., 2020; Conzuelo et al., 2012b; Eguílaz et al., 2010). The pH value of 6.0 (Conzuelo et al.,

TABLE 2 Experimental variables evaluated and optimized for immunosensor development.

Variable	Valuated interval	Selected value
CAb concentration	5–25	25 µg mL^{-1}
CAb incubation time	15–60	60 min
Number of steps	1–2	1 step
DAb-HRP concentration	0.05–1.0	0.5 µg mL^{-1}
DAb-HRP incubation time	15–60	60 min

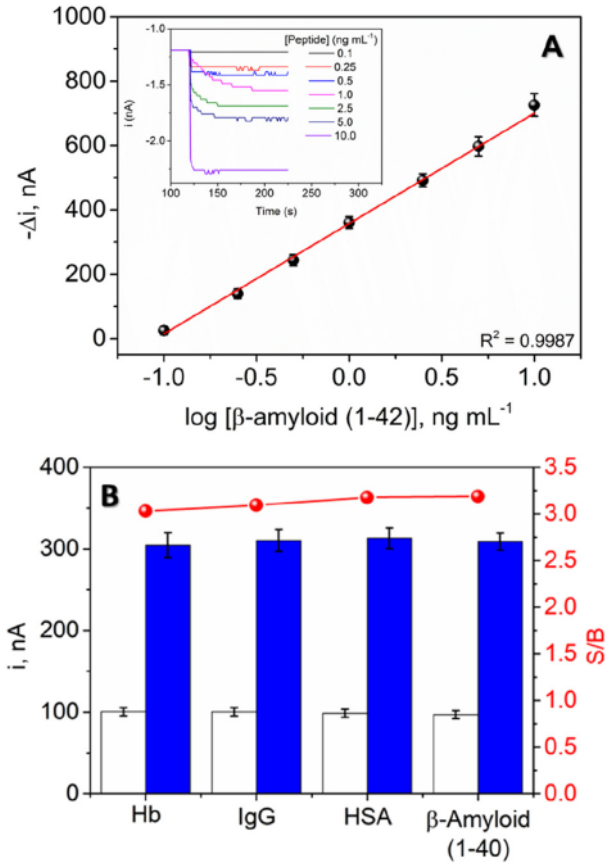

FIGURE 5
(A) Calibration curve generated for the amperometric determination of $A\beta_{1\text{-}42}$ using the immunosensor prepared with 25 µg mL^{-1} of the capture antibody (CAb). **(B)** Amperometric responses of the immunosensor for the concentrations of 0.0 (white bars) and 2.5 (blue bars) ng mL^{-1} of $A\beta_{1\text{-}42}$ in the presence of hemoglobin (Hb) (5.0 mg mL^{-1}), immunoglobulin G (IgG) (1.0 mg mL^{-1}), human serum albumin (HSA) (50.0 mg mL^{-1}), and β-amyloid (1–40) peptide (10.0 µg mL^{-1}).

TABLE 3 Main characteristics of electrochemical immunosensors for the determination of $A\beta_{1-42}$.

Sensor fundamentals	Approach/ Detection	Transduction technique	Analytical characteristics*	Preparation time	Sample	Reference
Au electrode modified with MNG and used for the immobilization of CAb	Direct immunosensor/ Label-free	DPV (Fe(CN)63−/4−)	L.R.: 0.005–0 ng mL^{-1} LOD: 5 pg mL−1	≈10 days	–	[33]
Highly conductive dual-layer of G and electrochemically rGO used for the immobilization of CAb	Direct immunosensor/ Label-free	DPV (Fe(CN)63−/4−)	L.R.: 0.050–248 ng mL^{-1} LOD: 10.8 pg mL−1	≈24 h	Human plasma Mice plasma	[34]
GCE/Au modified with PTH-MB, AuNPs, anti-Aβ42 and BSA	Competitive immunoassay using Aβ42 and heme-Aβ42	CV (H2O2/FcOH)	L.R.: 2.3–61.8 ng mL^{-1} LOD: 78.1 pg mL−1	≈19 h	Serum Saliva	[35]
Thin Au film on the 3D nanostructure PC substrate modified with AuNPs, MUA and CAb	Sandwich immunoassay using probe antibody	EIS (Fe(CN)63−/4−)	L.R.: 0.01–100 ng mL^{-1} LOD: 0.113 pg mL−1	≈31 h	–	[36]
ICE functionalized with SAM of MHA used for the immobilization of CAb	Direct immunosensor/ Label-free	Capacitance (non-Faradaic)	L.R.: 0.01–10 ng mL^{-1} LOD: 7.5 pg mL−1	≈14 h	Human serum	[37]
SPGEs modified with ultra-thin layers of pDAN used for the immobilization of CAb	Direct immunosensor/ Label-free	DPV (Fe(CN)63−/4−)	L.R.: 0.001–1 ng mL^{-1} LOD: 1.4 pg mL^{-1}	—	Human plasma	[38]
CAb immobilized on SPCE electrografted p-ABA	Direct immunosensor/ Label-free	EIS (Fe(CN)63−/4−)	L.R.: 1.0 × 10−6–0.1 ng mL−1 LOD: 3.84 × 10−3 pg mL^{-1}	3.5 h	–	[39]
GCE modified PtCoCu PNPs/NB-rGO used for the immobilization of CAb	Direct immunosensor/ Label-free	Amperometry (H2O2)	L.R.: 5.0 × 10−5–100 ng mL^{-1} LOD: 3.5 × 10−3 pg mL^{-1}	–	Human serum	[40]
MGN/Au electrode was used for immobilization of the specific peptide sequence	Peptide-based biosensor	DPV (Fe(CN)63−/4−)	L.R.: 0.003–7 ng mL^{-1} LOD: 0.2 pg mL^{-1}	–	Artificial CSF Serum	[41]
GCE modified with SNH and MPA used for the immobilization of CAb	Direct immunosensor/ Label-free	EIS (Fe(CN)63−/4−)	L.R.: 0.001–1 ng/mL^{-1} LOD: 6.38 × 10−4 pg mL^{-1}	>44 h	Human plasma	[42]
SPCE with sandwich immunoassay onto the MBs	Sandwich immunoassay using HRP-DAb	Amperometry (HQ/H2O2)	L.R.: 0.1–10 ng mL^{-1} LOD: 7.4 pg mL^{-1}	3.7 h	—	This work

*The conversion between units was performed considering the molecular weight of the $A\beta_{1-42}$ equal to 4,514.1 g mol^{-1}. $A\beta_{1-42}$: β-amyloid (1–42) peptide; Au: gold; AuNPs: gold nanoparticles; BSA: bovine serum albumin; CAb: capture antibody; CSF: cerebrospinal fluid; CV: cyclic voltammetry; DAb: detector antibody; DPV: differential pulse voltammetry; EIS: electrochemical impedance spectroscopy; GCE: glassy carbon electrode; GCE/Au: GCE with Au particles electrodeposited; HQ: hydroquinone; HRP: horseradish peroxidase; ICE: interdigitated chain-shaped electrode; LOD: limit of detection; L.R.: linear range; MBs: magnetic micro-beads; MGN: microporous gold nanostructure; MHA: 6-mercaptohexanoic acid; MNG: magnetic nitrogen doped graphene; MPA: mercaptopropionic acid; MUA: 11-mercaptoundecanoid acid; p-ABA: p-aminobenzoic acid; PC: polycarbonate; pDAN: polymerized 1,5-diaminonaphthalene; PtCoCu PNPs/NB-rGO: PtCoCu nanoparticles supported on N– and B–codoped rGO; PTH-MB: polythionine-methylene blue; rGO: reduced graphene oxide; SAM: self-assembled monolayer; SNF: electrospun SnO_2 nanofibers; SPGEs: screen printed graphene electrodes.

2012b) is consistent with the optimal pH range (6.0–6.5) for HRP enzyme activity (Ding et al., 2023). The tested ranges and selected values for each variable are summarized in Table 2, while Figure 4 illustrates the results.

In the development of an immunosensor, several important variables must be considered, including the consumption of immunoreagents, sensor preparation time, and sample analysis time. The goal is to minimize reagent consumption, shorten sensor preparation time, and achieve rapid analytical responses. In this study, a concentration of 25 μg mL^{-1} for the capture antibody (CAb) was selected, along with an incubation time of 60 min, based on the optimal signal-to-blank (S/B) ratios that provide the best efficiency for the analysis.

The number of steps required for assembling the immunosensor was determined by analyzing the results of two work protocols, both starting from the modification stage of the magnetic beads (MBs) with the capture antibody (CAb). Protocol one involved a single incubation step in a mixed solution containing $A\beta_{1-42}$ and DAb-HRP for 60 min (1 step). Protocol 2, on the other hand, included two successive incubation steps: first, with the standard $A\beta_{1-42}$ solution for 60 min, followed by incubation with the detection antibody conjugated with horseradish peroxidase (DAb-HRP) for another 60 min (2 steps). Figures 4–D shows that the best signal-to-background (S/B) ratio was achieved with Protocol 1 (a single step), likely due to the higher efficiency of biorecognition events occurring in a homogeneous mixture of antigens and antibodies.

Figures 4–E shows the effect of the concentration of the HRP-labeled detection antibody (DAb-HRP) on the response of the immunosensor. The signal-to-background ratio (S/B) increased with rising DAb-HRP concentrations up to 0.5 μg mL^{-1} but decreased at a concentration of 1.0 μg mL^{-1}. This decrease is attributed to the reduced specific response to $A\beta_{1\text{-}42}$ (S), indicating impaired molecular recognition, which may be caused by excessive amounts of DAb-HRP. As for the incubation time of the $A\beta_{1\text{-}42}$ + DAb-HRP mixture, an incubation period of 60 min was selected, as shown in Figures 4–F.

3.3 Calibration curves and determination of analytical parameters

The calibration curve for $A\beta_{1\text{-}42}$ was constructed using the immunosensor prepared with 25 μg mL^{-1} of the capture antibody (CAb) immobilized on the magnetic beads (MBs) (Figures 5–A).

Figure 5A shows that the response current of the immunosensor exhibits an increasing linear relationship with the logarithm of the $A\beta_{1\text{-}42}$ concentration, in a concentration range of 100 to 10,000 pg mL^{-1} according to the equation: $-\Delta i$ (nA) = (357.5 ± 5.2) + (342.8 ± 7.8) log[$A\beta_{1\text{-}42}$] (ng mL^{-1}). The limit of detection (LOD) was calculated according to formula 3 × Sb/m, where Sb represents the standard deviation of the arithmetic mean of the measurements of 10 blanks, and m is the slope value of the analytical curve. The immunosensor has an LOD of 7.4 pg mL^{-1}, a value consistent with the values reported in the literature (Table 3) for electrochemical immunosensors. When compared to the lower reference limit for $A\beta_{1\text{-}42}$ in cerebrospinal fluid (CSF) (192 pg mL^{-1}), the response of the immunosensor is significantly lower. Consequently, the immunosensor is suitable for the detection of Alzheimer's disease, given that the onset of the pathology occurs when CSF-$A\beta_{1\text{-}42}$ drops below this threshold of 192 pg mL^{-1} (Ding et al., 2023).

Selectivity is a crucial parameter for the application of the proposed immunosensor in clinical plasma or cerebrospinal fluid (CSF) samples. The selectivity of the immunosensor was evaluated against several proteins potentially found in plasma and CSF samples, including human IgGs, hemoglobin (Hb), human serum albumin (HSA), and β-amyloid peptide (1–40). The tests were conducted by measuring $A\beta_{1\text{-}42}$ concentrations of 0.0 and 2.5 ng mL^{-1} both in the absence and in the presence of these interferents, at concentrations equivalent to those found in the serum of healthy individuals. The presence of these interferents did not affect the determination of $A\beta_{1\text{-}42}$, as shown in Figures 5–B.

The developed immunosensor was prepared in 4 h, without involving exhaustive synthesis procedures, demonstrating good reproducibility (RSD of 4.7%) and stability. Reproducibility measurements were performed for the concentration of 500 pg mL^{-1} of $A\beta_{1\text{-}42}$ using 8 identically prepared immunosensors tested on the same day. For interday stability measurements, the immunosensors were prepared from CAb-MBs stored in filtered PBS at 4°C for at least 15 days, and no significant difference was observed in the signal-to-noise (S/B) ratio for measurements of 0.0 and 500 pg mL^{-1} of $A\beta_{1\text{-}42}$.

4 Conclusion

An amperometric immunosensor based on magnetic microspheres modified with sandwich-type immunocomplexes was developed for the detection of $A\beta_{1\text{-}42}$. Magnetic microbeads functionalized with –COOH groups were used as the platform for the construction of the immunosensor. The construction steps of the immunosensor were characterized by DLS, zeta potential measurements, TEM, FTIR, and Raman spectroscopy, and confirmed the modifications that occur on the surface of the microparticles and the biorecognition of the @peptide-DAb-HRP complex by the capture antibody covalently immobilized on the MBS. The experimental variables were optimized, and the analytical characteristics of the immunosensor were determined, showing a linear amperometric response in the range of 0.1–10 ng mL^{-1} and a limit of detection (LOD) of 7.4 pg mL^{-1}. Furthermore, the immunosensor exhibited good reproducibility, stability, and selectivity for IgG, hemoglobin (Hb), human serum albumin (HSA), and β-amyloid peptide (1–40). The developed immunosensor is suitable for detecting Alzheimer's disease (AD) in cerebrospinal fluid (CSF) samples in a cost-effective, rapid, and simple manner. This methodology does not require material synthesis or electrode modifications, as the sensor interface is directly and rapidly constructed on commercial magnetic microspheres.

Data availability statement

The original contributions presented in the study are included in the article/Supplementary Material, further inquiries can be directed to the corresponding author.

Author contributions

CR: Conceptualization, Data curation, Formal Analysis, Investigation, Methodology, Validation, Writing–original draft, Writing–review and editing. LS: Conceptualization, Methodology, Writing–original draft, Writing–review and editing. JC-B: Conceptualization, Formal Analysis, Investigation, Methodology, Writing–original draft, Writing–review and editing. AZ: Investigation, Writing–original draft, Writing–review and editing. CC: Formal Analysis, Visualization, Writing–original draft, Writing–review and editing. VZ: Supervision, Writing–original draft, Writing–review and editing. LV: Writing–original draft, Writing–review and editing. AL: Conceptualization, Funding acquisition, Project administration, Supervision, Writing–original draft, Writing–review and editing.

Funding

The author(s) declare that financial support was received for the research, authorship, and/or publication of this article. The authors would like to thank the São Paulo Research Foundation (FAPESP, #2015/26651-3 to CR), Coordination for the Improvement of Higher Education Personnel (CAPES) and

National Council for Scientific and Technological Development (CNPq, #310883/2020-2 to AL and #383239/2022-2 to AZ) for the support granted.

Conflict of interest

The authors declare that the research was conducted in the absence of any commercial or financial relationships that could be construed as a potential conflict of interest.

The author(s) declared that they were an editorial board member of Frontiers, at the time of submission. This had no impact on the peer review process and the final decision.

Generative AI statement

The author(s) declare that no Generative AI was used in the creation of this manuscript.

Publisher's note

References

Alex, W., and Gunn, R. N. (2019). Amyloid load: a more sensitive biomarker for amyloid imaging. *J. Nucl. Med.* 60, 536–540. doi:10.2967/jnumed.118.210518

Boelens, P., Bobeth, C., Hinman, N., Weiss, S., Zhou, S., Vogel, M., et al. (2022). Peptide functionalized Dynabeads for the magnetic carrier separation of rare-earth fluorescent lamp phosphors. *J. Magn. Magn. Mater* 563, 169956. doi:10.1016/j.jmmm.2022.169956

Brazaca, L. C., Sampaio, I., Zucolotto, V., and Janegitz, B. C. (2020). Applications of biosensors in Alzheimer's disease diagnosis. *Talanta* 210, 120644. doi:10.1016/j.talanta.2019.120644

Breydo, L., Kurouski, D., Rasool, S., Milton, S., Wu, J. W., Uversky, V. N., et al. (2016). Structural differences between amyloid beta oligomers. *Biochem. Biophys. Res. Commun.* 477, 700–705. doi:10.1016/j.bbrc.2016.06.122

Burt, J. L., Gutiérrez-Wing, C., Miki-Yoshida, M., and José-Yacamán, M. (2004). Noble-metal nanoparticles directly conjugated to globular proteins. *Langmuir* 20, 11778–11783. doi:10.1021/la048287r

Byun, C. K. (2016). Investigation of chemical modification on tosyl-activated polystyrene microsphere magnetic particle surface by infrared microscopy. *Anal. Sci. Technol.* 29, 225–233. doi:10.5806/AST.2016.29.5.225

Camacho, C., Matías, J. C., Chico, B., Cao, R., Gómez, L., Simpson, B. K., et al. (2007). Amperometric biosensor for hydrogen peroxide, using supramolecularly immobilized horseradish peroxidase on the β-cyclodextrin-coated gold electrode. *Electroanalysis* 19, 2538–2542. doi:10.1002/elan.200703993

Chen, M., McReynolds, N., Campbell, E. C., Mazilu, M., Barbosa, J., Dholakia, K., et al. (2015). The use of wavelength modulated Raman spectroscopy in label-free identification of T lymphocyte subsets, natural killer cells and dendritic cells. *PLoS One* 10, e0125158. doi:10.1371/journal.pone.0125158

Conzuelo, F., Gamella, M., Campuzano, S., Pinacho D, G., Reviejo, A. J., Marco, M. P., et al. (2012b). Disposable and integrated amperometric immunosensor for direct determination of sulfonamide antibiotics in milk. *Biosens. Bioelectron.* 36, 81–88. doi:10.1016/j.bios.2012.03.044

Conzuelo, F., Gamella, M., Campuzano, S., Reviejo, A. J., and Pingarrón, J. M. (2012a). Disposable amperometric magneto-immunosensor for direct detection of tetracyclines antibiotics residues in milk. *Anal. Chim. Acta* 737, 29–36. doi:10.1016/j.aca.2012.05.051

Ding, M., Ding, S., Du, D., Wang, X., Hu, X., Guan, P., et al. (2023). Recent advances in electrochemical biosensors for the detection of Aβ42, a biomarker for Alzheimer disease diagnosis. *Trends Anal. Chem.* 164, 117087. doi:10.1016/j.trac.2023.117087

Eguílaz, M., Moreno-Guzmán, M., Campuzano, S., González-Cortés, A., Yáñez-Sedeño, P., and Pingarrón, J. M. (2010). An electrochemical immunosensor for testosterone using functionalized magnetic beads and screen-printed carbon electrodes. *Biosens. Bioelectron.* 26, 517–522. doi:10.1016/j.bios.2010.07.060

Findeis, M. A. (2007). The role of amyloid β peptide 42 in Alzheimer's disease. *Pharmacol. Ther.* 116, 266–286. doi:10.1016/j.pharmthera.2007.06.006

Gamella, M., Bueno-Díaz, C., Ruiz-Valdepeñas Montiel, V., Povedano, E., Reviejo, A. J., Villalba, M., et al. (2020). First electrochemical immunosensor for the rapid detection of mustard seeds in plant food extracts. *Talanta* 219, 121247. doi:10.1016/j.talanta.2020.121247

Gamella, M., Campuzano, S., Conzuelo, F., Reviejo, A. J., and Pingarrón, J. M. (2012). Amperometric magnetoimmunosensors for direct determination of D-dimer in human serum. *Electroanalysis* 24, 2235–2243. doi:10.1002/elan.201200503

Guivernau, B., Bonet, J., Valls-Comamala, V., Bosch-Morató, M., Godoy, J. A., Inestrosa, N. C., et al. (2016). Amyloid-β peptide nitrotyrosination stabilizes oligomers and enhances NMDAR-mediated toxicity. *J. Neurosci.* 36, 11693–11703. doi:10.1523/jneurosci.1081-16.2016

Imanbekova, M., Suarasan, S., Rojalin, T., Mizenko, R. R., Hilt, S., Mathur, M., et al. (2021). Identification of amyloid beta in small extracellular vesicles via Raman spectroscopy. *Nanoscale Adv.* 3, 4119–4132. doi:10.1039/d1na00330e

Ishigaki, M., Morimoto, K., Chatani, E., and Ozaki, Y. (2020). Exploration of insulin amyloid polymorphism using Raman spectroscopy and imaging. *Biophys. J.* 118, 2997–3007. doi:10.1016/j.bpj.2020.04.031

Le, H. T. N., Park, J., and Cho, S. (2020). A probeless capacitive biosensor for direct detection of amyloid beta 1-42 in human serum based on an interdigitated chain-shaped electrode. *Micromachines* 11, 791. doi:10.3390/mi11090791

Michael, R., Otto, C., Lenferink, A., Gelpi, E., Montenegro, G. A., Rosandić, J., et al. (2014). Absence of amyloid-beta in lenses of Alzheimer patients: a confocal Raman microspectroscopic study. *Exp. eye Res.* 119, 44–53. doi:10.1016/j.exer.2013.11.016

Miller, L. M., Bourassa, M. W., and Smith, R. J. (2013). FTIR spectroscopic imaging of protein aggregation in living cells. *Biochim. Biophys. Acta Biomembr.* 1828, 2339–2346. doi:10.1016/j.bbamem.2013.01.014

Moran, S. D., and Zanni, M. T. (2014). How to get insight into amyloid structure and formation from infrared spectroscopy. *J. Phys. Chem. Lett.* 5, 1984–1993. doi:10.1021/jz500794d

Sarroukh, R., Goormaghtigh, E., Ruysschaert, J.-M., and Raussens, V. (2013). ATR-FTIR: a "rejuvenated" tool to investigate amyloid proteins. *Biochim. Biophys. Acta Biomembr.* 1828, 2328–2338. doi:10.1016/j.bbamem.2013.04.012

Serafín, V., Gamella, M., Pedrero, M., Montero-Calle, A., Razzino, C. A., Yáñez-Sedeño, P., et al. (2020). Enlightening the advancements in electrochemical bioanalysis for the diagnosis of Alzheimer's disease and other neurodegenerative disorders. *J. Pharm. Biomed. Anal.* 189, 113437. doi:10.1016/j.jpba.2020.113437

Shui, B., Tao, D., Florea, A., Cheng, J., Zhao, Q., Gu, Y., et al. (2018). Biosensors for Alzheimer's disease biomarker detection: a review. *Biochimie* 147, 13–24. doi:10.1016/j.biochi.2017.12.015

Toyos-Rodríguez, C., García-Alonso, F. J., and de la Escosura-Muñiz, A. (2020). Electrochemical biosensors based on nanomaterials for early detection of Alzheimer's disease. *Sensors* 20, 4748. doi:10.3390/s20174748

van Apeldoorn, A., Aksenov, Y., Stigter, M., Hofland, I., de Bruijn, J., Koerten, H., et al. (2005). Parallel high-resolution confocal Raman SEM analysis of inorganic and organic bone matrix constituents. *J. R. Soc. Interface* 2, 39–45. doi:10.1098/rsif.2004.0018

Volpe, G., Compagnone, D., Draisci, R., and Palleschi, G. (1998). 3,3′,5,5′-Tetramethylbenzidine as electrochemical substrate for horseradish peroxidase based enzyme immunoassays: a comparative study. *Analyst* 123, 1303–1307. doi:10.1039/a800255j

Wang, P.-G., Li, B.-R., Wang, Y.-L., Wu, C.-C., and Chen, J.-C. (2023). Application of aminobenzoic acid electrodeposited screen-printed carbon electrode in the beta-amyloid electrochemical impedance spectroscopy immunoassay. *Talanta* 254, 124154. doi:10.1016/j.talanta.2022.124154

WHO (2017). *Global action plan on the public health response to dementia 2017 - 2025*. Geneva: World Health Organization. Available at: https://apps.who.int/iris/bitstream/handle/10665/259615/9789241513487-eng.pdf;jsessionid=4DA480FA93471AC53988E52B35F416D8?sequence=1 (Accessed June 25, 2023).

Zandomeneghi, G., Krebs, M. R., McCammon, M. G., and Fändrich, M. (2004). FTIR reveals structural differences between native β-sheet proteins and amyloid fibrils. *Protein Sci.* 13, 3314–3321. doi:10.1110/ps.041024904

Zaretsky, D. V., Zaretskaia, M. V., and Molkov, Y. I. (2022). Patients with Alzheimer's disease have an increased removal rate of soluble beta-amyloid-42. *PLoS One* 17, e0276933. doi:10.1371/journal.pone.0276933